Engineering and functional analysis of yeast with a monotypic 40S ribosome subunit

Xin Hu[a,1], Shuangying Jiang[b,1], Feifei Xu[c,1], Cheng Zeng[b], Xiangxiang Wang[a], Wei Liu[d], Aimin Cheng[e], Chengying Ma[e], Ning Gao[e], Yuyu Zhao[a], Junbiao Dai[b,2], and Guanghou Zhao[a,2]

[a]School of Ecology and Environment, Northwestern Polytechnical University, Xi'an 710129, China; [b]CAS Key Laboratory of Quantitative Engineering Biology, Guangdong Provincial Key Laboratory of Synthetic Genomics and Shenzhen Key Laboratory of Synthetic Genomics, Shenzhen Institute of Synthetic Biology, Shenzhen Institutes of Advanced Technology, Chinese Academy of Sciences, Shenzhen 518055, China; [c]Department of Anesthesiology and Perioperative Medicine, Xijing Hospital, Fourth Military Medical University, Xi'an 710032, China; [d]State Key Laboratory of Genetic Resources and Evolution, Kunming Institute of Zoology, Chinese Academy of Sciences, Kunming 650223, China; and [e]State Key Laboratory of Membrane Biology, Peking-Tsinghua Center for Life Sciences, School of Life Sciences, Peking University, Beijing 100871, China

Edited by Jens Nielsen, BioInnovation Institute, DK2200 Copenhagen, Denmark; received August 6, 2021; accepted December 21, 2021

Emerging evidence reveals that ribosomes are not monolithic but dynamic machines with heterogeneous protein compositions that can reshape ribosomal translational abilities and cellular adaptation to environmental changes. Duplications of ribosomal protein (RP) genes are ubiquitous among organisms and are believed to affect cell function through paralog-specific regulation (e.g., by generating heterogeneous ribosomes) and/or gene dose amplification. However, direct evaluations of their impacts on cell function remain elusive due to the highly heterogeneous cellular RP pool. Here, we engineered a yeast with homogeneous 40S RP paralog compositions, designated homo-40S, by deleting the entire set of alternative duplicated genes encoding yeast 40S RP paralogs. Homo-40S displayed mild growth defects along with high sensitivity to the translation inhibitor paromomycin and a significantly increased stop codon readthrough. Moreover, doubling of the remaining RP paralogous genes in homo-40S rescued these phenotypes markedly, although not fully, compared to the wild-type phenotype, indicating that the dose of 40S RP genes together with the heterogeneity of the contents was vital for maintaining normal translational functionalities and growth robustness. Additional experiments revealed that homo-40S improved paromomycin tolerance via acquisition of bypass mutations or evolved to be diploid to generate fast-growing derivatives, highlighting the mutational robustness of engineered yeast to accommodate environmental and genetic changes. In summary, our work demonstrated that duplicated RP paralogs impart robustness and phenotypic plasticity through both gene dose amplification and paralog-specific regulation, paving the way for the direct study of ribosome biology through monotypic ribosomes with a homogeneous composition of specific RP paralogs.

heterogenous ribosomes | ribosomal protein paralogs | CRISPR/Cas9 | paromomycin sensitivity

Eukaryotic ribosomes are highly complex protein synthesis machinery composed of the small/40S subunit and the large/60S subunit. Historically, the ribosome was considered to be an invariant effector rather than a regulatory participant in translation. However, emerging studies have revealed heterogeneity among ribosomes, characterized by variable ribosomal protein (RP) contents and consequent specialization of the translational program for modulating growth robustness and stress response (1–4). Such findings led to the formulation of the concept of "specialized ribosomes", wherein multiple populations of ribosomes with diverse compositions were produced, and each was tailored to carry different translational abilities, such as mRNA selectivity during translation as well as translation fidelity and elongation speed (5–7). Although current evidence proves the existence of ribosome heterogeneity and the functional specialization for distinct ribosomes in selectively translating specific subsets of messenger RNAs (mRNAs), the sources of ribosome heterogeneity and thereafter the output remain largely unknown and are subjects of great interest (5–7).

In both lower and higher eukaryotes, many RPs are encoded by paralogous genes, possibly originating from genome duplication early in evolution and maintained afterward (7–9). For example, 24 of the 33 RPs in the yeast 40S ribosome subunit, which contains the ribosome decoding center, exist as paralog pairs, which allows 2^{24} ($>10^7$) potential RP combinations by numbers alone. To date, numerous studies have examined the roles of individual RP paralogs in diverse organisms (e.g., yeast, amoebas, flies, and vertebrates), and, accordingly, rapidly growing evidence has shown that RP paralog pairs usually possess distinct or even opposite expression patterns and paralog-specific functions (10–12). Thus, heterogeneous RP paralogs not only regulate cell function by complementing each other's expression levels (dose amplification) but also offer the potential to generate heterogeneous ribosomes by swapping distinct RP isoforms to fine-tune the translational program (paralog-specific regulation) (2, 10–12). However, direct evaluation of their effects on cell function, especially the functionalities of ribosomes, was obscured by the highly diversified cellular RP pool (5, 6).

Significance

Ribosomes are not monolithic but dynamic machines composed of heterogeneous ribosomal protein (RP) paralogs with elusive functions. Isolation and characterization of monotypic ribosomes with homogeneous RP paralog compositions represent ideal approaches to understand the role of pervasive RP paralogs in customizing translation abilities but are largely hurdled by the complexity of the cellular ribosome pool (e.g., in *Saccharomyces cerevisiae*, 59 RP paralog pairs allow $>10^{17}$ potential RP combinations). Here, we engineered a yeast with monotypic 40S ribosomes, including both defined and homogenous RP paralogs, and further functional studies revealed that duplicated RP paralogs impart robustness and phenotypic plasticity (such as paromomycin tolerance) through both gene dose amplification and paralog-specific regulation, paving a way for the study of monotypic ribosomes.

Author contributions: X.H., S.J., F.X., J.D., and G.Z. designed research; X.H., S.J., F.X., C.Z., X.W., W.L., A.C., C.M., Y.Z., and G.Z. performed research; X.H., S.J., F.X., C.Z., X.W., W.L., N.G., J.D., and G.Z. analyzed data; and X.H., S.J., F.X., J.D., and G.Z. wrote the paper.

The authors declare no competing interest.

This article is a PNAS Direct Submission.

[1]X.H., S.J., and F.X. contributed equally to this work.

[2]To whom correspondence may be addressed. Email: junbiao.dai@siat.ac.cn or zhaogh@nwpu.edu.cn.

This article contains supporting information online at http://www.pnas.org/lookup/suppl/doi:10.1073/pnas.2114445119/-/DCSupplemental

Published February 1, 2022.

In this study, we homogenized the cellular 40S RP pool by removing one set of paralogous genes and consequently constructed a "designer" yeast named homo-40S. Although the successful engineering of homo-40S demonstrated that the presence of duplicated RP paralogs was not essential for yeast survival, our results showed that loss of RP paralogs in homo-40S led to decreased fitness and increased susceptibility to the translation error-inducing inhibitor paromomycin, which is indicative of altered translational activity and fidelity. Moreover, these phenotypes could be recovered markedly, although not fully, by doubling the RP paralogous genes in homo-40S. Furthermore, our study showed that homo-40S was able to improve paromomycin tolerance via acquisition of bypass mutations or evolved to be diploid to acquire fast-growing derivatives. Together, our work provides a strategy to acquire monotypic ribosomes with homogenized RP contents and experimentally demonstrates the functional significance for maintaining duplicated RP genes.

Results

Construction of Homo-40S via Iterative Cas9-Mediated Evolution (iCasEvo). The construction of homo-40S required the iterative deletion of 24 RP genes (Fig. 1*A*). First, highly efficient multiplex gene substitution was achieved through a modified CRISPR–Cas9 system with guide RNA (gRNA)-donor editing cassettes derived from robust homologous recombination (gap repair) of delivered editing elements (*SI Appendix*, Fig. S1 *A–E*) (13). Although the CRISPR–Cas9 system is a highly efficient and ready-to-use genome-editing tool, current iterative genome-editing methods include essential steps to eliminate the previous gRNA-expressing plasmids before another gRNA-expressing plasmid can be introduced. Thus, we designed a plasmid elimination element (PEE) consisting of a galactose-inducible 2μ-targeted gRNA-expressing cassette, which would cleave and eliminate the gRNA-expressing plasmids upon galactose induction with high efficiency (>95%) to facilitate editing cassette swaps (Fig. 1*B* and *SI Appendix*, Fig. S1 *A* and *F*). Then, we combined both the CRISPR–Cas9 system for gene editing and inducible PEE for iterative genome editing, and we refer to this method as iCasEvo.

Then, to avoid potential severe fitness defects or even lethality caused by RP gene deletion, "subordinate" paralogous genes, based on previous reports of the essentiality of each paralog, were carefully selected for deletion, which mainly caused moderate growth rate loss (Fig. 1*A*) (14, 15). Moreover, strain growth was investigated per gene deletion cycle during strain construction to monitor the potential fitness loss and accordingly modify the design to meet fitness requirements (*SI Appendix*, Fig. S2). Ultimately, the engineered strains were verified by combinatorial approaches to avoid confounding results (see below).

With iCasEvo, we carried out 14 successive rounds of gene editing and successfully constructed homo-40S (Fig. 2). PCR analysis was used to validate homo-40S. The engineered strain showed smaller amplicons than the wild-type strain at the corresponding loci because of the deletion of particular RP genes (Fig. 2*A*). The pulsed-field gel electrophoresis results showed that homo-40S possesses a normal karyotype (Fig. 2*B*). To further identify theoretical and nontargeted changes during strain construction, whole-genome sequencing (WGS) analysis was performed, which revealed that in addition to the expected gene deletion, 40 nontargeted single-nucleotide polymorphisms (SNPs) were also detected in homo-40S (Dataset S1), presumably derived from random mutations (16).

Homo-40S Fitness Loss. To investigate the consequence of deleting the 24 40S RP paralogs, we evaluated the phenotypic changes of homo-40S cells. The size and morphology of homo-40S and wild-type (hetero-40S) cells were similar (Fig. 2*C*). However, the homo-40S cells displayed a reduction in growth fitness on different complete medium with various carbon sources and under several other stresses except for NaCl treatment (Fig. 2 *D* and *E* and *SI Appendix*, Fig. S3). RNA sequencing analysis revealed that there were only mild perturbations in homo-40S (*SI Appendix*, Fig. S4). Overall, 150 genes were significantly influenced by deletion of the RP genes, of which 100 were down-regulated and 50 were up-regulated (*SI Appendix*, Fig. S4 and Dataset S3). As expected, of the 100 down-regulated genes, 24 genes encoded 40S RPs (marked blue). Then, the other 126 significantly affected genes were analyzed

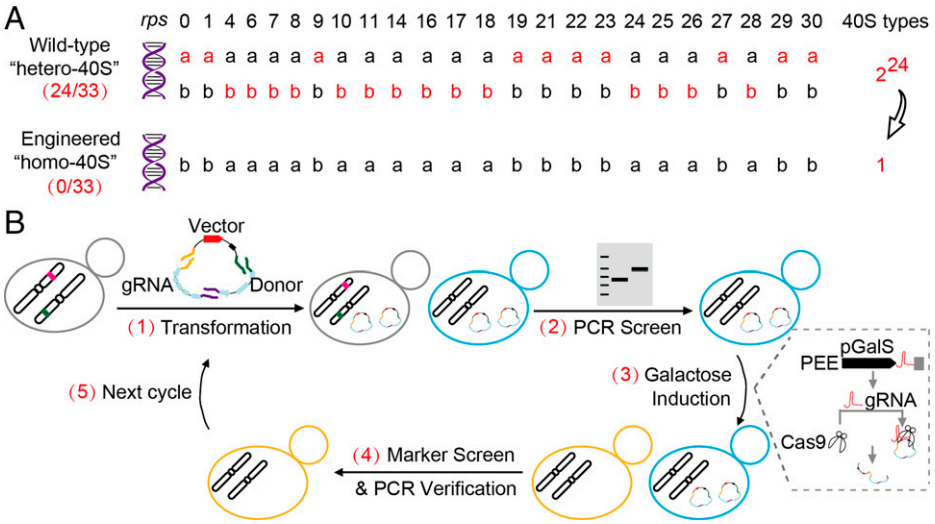

Fig. 1. Design and workflow for engineering homo-40S. (*A*) In *S. cerevisiae*, 24 of 33 RPs comprising the 40S ribosomal subunit exist as paralog pairs, and this allows 2^{24} (>10^7) potential RP combinations. RP isoforms deleted in homo-40S are marked in red. (*B*) Workflow for iCasEvo. First, separative gRNA/donor/vector cassettes (see details in *SI Appendix*, Fig. S1) were gap repaired by the yeast homologous recombination system and evoked gene editing; second, strains with targeted gene deletion/substitution were picked; third, picked strains were induced to eradicate the editing cassettes by the PEE. In the PEE (as shown in the circle marked with dashed lines, or see more detail in *SI Appendix*, Fig. S1*A* and Dataset S2), the 2μ-targeted gRNA was driven by a galactose-inducible GalS promoter (pGalS) and would guide Cas9 nuclease to cleave and eliminate the 2μ plasmids expressing editing cassettes upon galactose induction; finally, strains without editing cassettes as marked by loss of marker genes in the 2μ plasmids were isolated and further analyzed by PCR to verify the designed gene deletion, which thereafter were ready for the next round of gene editing.

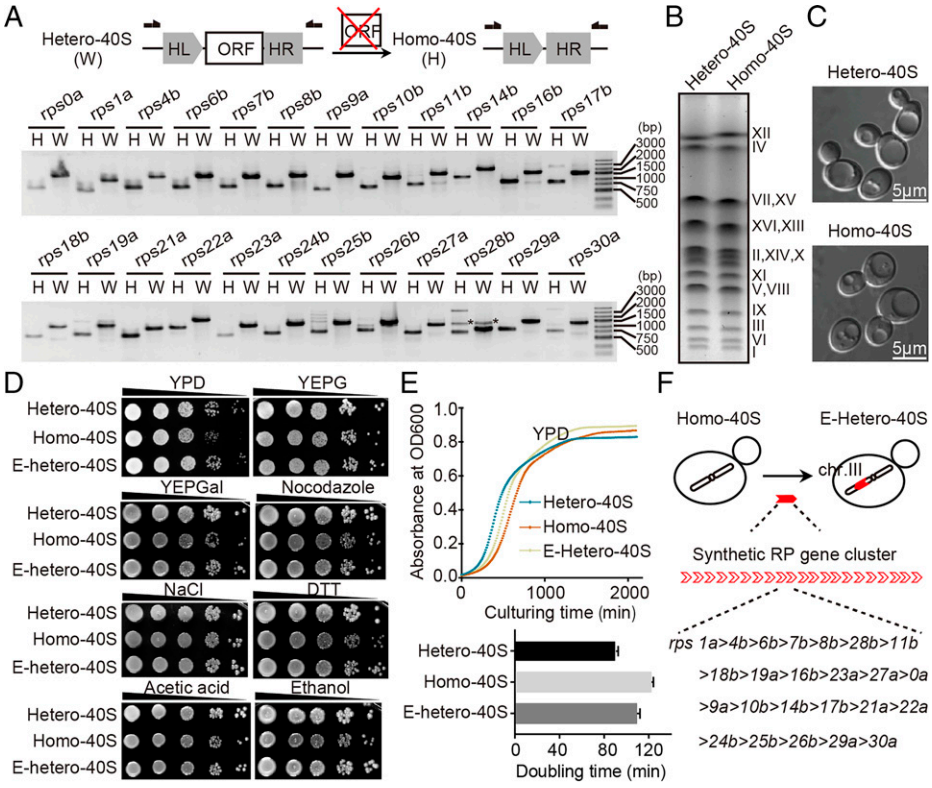

Fig. 2. Homo-40S exhibits loss of growth fitness. (*A*) PCR analysis of BY4741 (hetero-40S/W) and homo-40S (H); HL or HR, homologous arms in donor cassettes; ORF, open reading frame. The asterisks (*) mark nonspecific amplification bands. (*B*) Pulsed-field gel electrophoresis for chromosomal DNA analysis. (*C*) Cell morphology was analyzed by confocal microscope, and representative images are shown. (*D*) Fitness analysis of wild-type hetero-40S, synthetic homo-40S, and E-hetero-40S under nutrient-rich or several stress conditions. (*E*) Growth curves (*Top*) and doubling time (mean ± SD; *Bottom*) of hetero-40S, homo-40S, and E-hetero-40S in YPD medium. Growth curves are shown by the mean of four biological replicates of each strain. (*F*) A schematic showing a synthetic RP gene cluster designed to introduce 24 deleted RP genes back into homo-40S; chr, chromosome.

for significantly enriched Gene Ontology (GO) categories. Only genes involved in carbohydrate metabolic/biosynthetic processes were enriched in the down-regulated mRNA subsets (Dataset S3), indicating a perturbation of cellular energy metabolism, which could be related to the impaired growth fitness of homo-40S. Together, the transcriptomic analysis revealed additional levels of deficiency in homo-40S.

To delineate whether such phenotypic changes in homo-40S were attributed to the deletion of RP genes or nontargeted changes acquired during strain construction, we designed and constructed a synthetic gene cluster containing all of the wild-type RP genes (including introns), which were deleted in homo-40S (Fig. 2*F*). Furthermore, this engineered gene cluster was introduced back into homo-40S at an ectopic locus that was tolerant to insertion of a large DNA fragment (17); we referred to this strain as E-hetero-40S. E-hetero-40S therefore possessed not only nontargeted changes in homo-40S but also the same set of 40S ribosomal proteins as the wild-type strain (*SI Appendix*, Fig. S5). As expected, E-hetero-40S showed obviously improved growth compared to homo-40S (Fig. 2*F*), although it was not fully functional compared to the hetero-40S, which might be explained by the RP expression deviations in between the ectopic gene cluster and the endogenous loci (*SI Appendix*, Fig. S6).

Taken together, our experimental results demonstrated that the monotypic 40S ribosome subunit can support cell viability, and loss of the additional set of RP paralogs results in unambiguous negative effects on growth fitness.

Homo-40S Exhibits Altered Translational Functionalities. To evaluate the influence of the systematic RPs changes in homo-40S on global gene expression, global translation activity was assessed by puromycin incorporation, which could be detected by Western blot (18). As shown in Fig. 3*A*, homo-40S displayed puromycin incorporation signals comparable to those of the wild-type strain (hetero-40S), demonstrating that homo-40S did not possess obvious defects in global protein synthesis. To further investigate possible consequences caused by RPs changes in translation, homo-40S was treated with a variety of translation inhibitors, including anisomycin, hygromycin B, and paromomycin (19, 20). We found that homo-40S was only mildly sensitive to hygromycin B and was insensitive to anisomycin (Fig. 3*B*). In contrast, homo-40S was hypersensitive to paromomycin, which binds to the decoding center of the 40S ribosome subunit and induces translational inhibition as well as translational errors (19–21). The hypersensitivity of homo-40S to paromomycin was further verified in a puromycin incorporation assay. Although paromomycin treatment attenuated global protein synthesis in both hetero-40S and homo-40S, homo-40S displayed more severe translational inhibition than hetero-40S (Fig. 3*A*). Furthermore, translational fidelity was evaluated using a dual-luciferase reporter assay system (19). In this system, various modifications were introduced into the fusion protein of Renilla luciferase (Rluc) and Firefly luciferase (Fluc) so that different types of translational error can be quantified, such as stop codon readthrough and amino acid misincorporation (19, 22–24). With these reporters, we found that although no significant changes in amino acid misincorporation rates were observed, homo-40S had significantly increased rates of stop codon readthrough, indicating that the translational fidelity of homo-40S was altered.

In summary, these results revealed that systematic inactivation of alternative 40S RP paralogs impaired translation, as evident

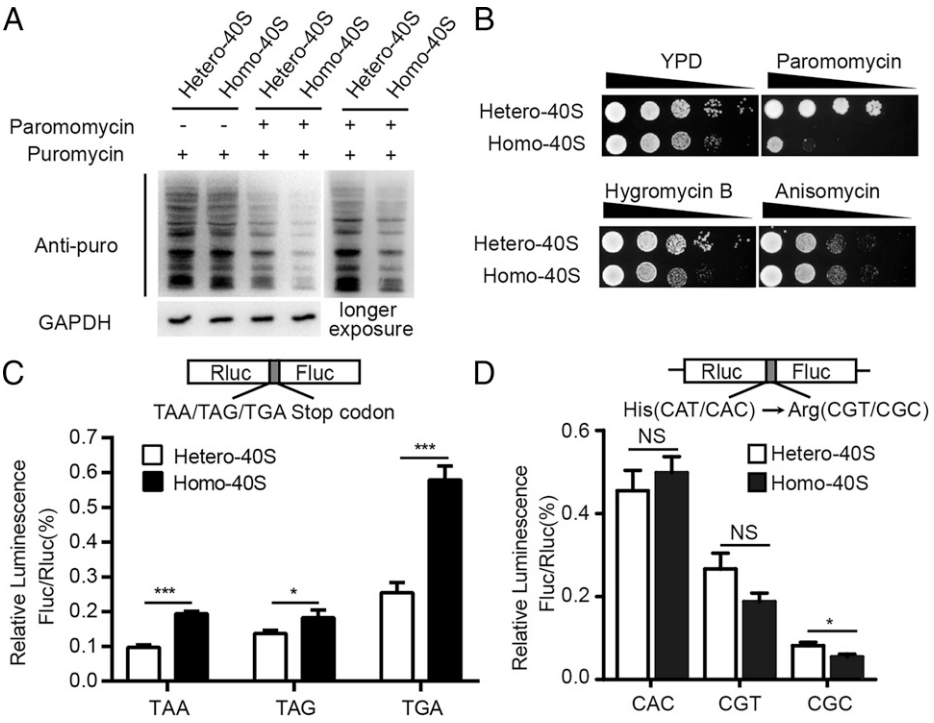

Fig. 3. Homo-40S exhibits altered translational functionalities. (*A*) Global translation activity was measured by puromycin incorporation in the presence or absence of paromomycin. Neosynthesized proteins were labeled with puromycin and analyzed by immunoblotting with an antibody against puromycin. GAPDH is shown as a loading control. (*B*) Serial dilution assays under the translational inhibitors (paromomycin, hygromycin B, and anisomycin) with wild-type (hetero-40S) and homo-40S. (*C* and *D*) The translation fidelity of wild-type (hetero-40S) and homo-40S was evaluated with reporters containing an insertion of a stop codon (TAA/TAG/TGA) between Rluc and Fluc or by amino acid misincorporation. Values are represented as means ± SD (*t* test; ***$P < 0.001$; *$P < 0.05$; $n \geq 3$).

by the substantially increased susceptibility of homo-40S to the translational inhibitor paromomycin as well as the altered parameters of translational activity and fidelity in homo-40S.

Doubling of Retained RP Paralogous Genes in Homo-40S Markedly Rescues Fitness and Translational Functionalities. Models of duplicated gene evolution posit that duplicated genes were maintained across evolution to impart robustness and phenotypic plasticity through gene dose amplification, partitioning of ancestral functions (subfunctionalization), acquisition of novel functions (neofunctionalization), or a combination of these changes (25). Indeed, polyribosome profile analysis revealed that, compared to the wild-type hetero-40S, homo-40S showed obviously decreased amounts of 40S subunits, overaccumulation of 60S subunits, and substantially reduced levels of 80S ribosomes and polysomes (Fig. 4*A*), representing a shortage of 40S subunits in homo-40S. To test whether such phenotypic alterations of homo-40S were generated by the gene dose effect, a synthetic gene cluster containing an extra copy of retained 40S RP paralogous genes was introduced into homo-40S, and this engineered strain was referred to as E-homo-40S (Fig. 4*B*). Accordingly, E-homo-40S held the same 40S RP gene number as the wild type but lost the wild-type heterogeneous 40S RP contents. RNA sequencing analysis confirmed that 40S RP mRNAs were increased in E-homo-40S compared with homo-40S (*SI Appendix*, Fig. S7). Consistent with this, polysome profile analysis revealed that there were obviously increased amounts of 40S subunits and polysomes as well as decreased accumulation of 60S subunits in E-homo-40S compared with homo-40S (Fig. 4*A*), representing that doubling of retained RP paralogous genes in homo-40S increased the doses of mature ribosomes. Next, we monitored the growth robustness and translational abilities of E-homo-40S. Compared to homo-40S, E-homo-40S demonstrated obviously improved growth robustness, although it was not fully functional compared to the wild type (Fig. 4*C* and *SI Appendix*, Fig. S8). In addition, a puromycin incorporation assay showed that E-homo-40S displayed substantially increased translational activity upon paromomycin treatment, which was consistent with the rescued tolerance to paromomycin of E-homo-40S (Fig. 4 *C* and *D*). Moreover, the significantly increased rates of stop codon readthrough observed in homo-40S were restored to wild-type levels in E-homo-40S (Fig. 4*E*). Taken together, our results showed that doubling of the remaining RP paralogous genes of homo-40S was able to partially compensate for the systematic disruption of their paralogous pairs, indicating that the gene dose of 40S RP was vital for maintaining cellular robustness.

Homo-40S Adapts Paromomycin Exposure via Acquisition of Bypass Mutations. Interestingly, homo-40S frequently produced larger colonies distinguished from slower-than-normal background populations when cultured in paromomycin-containing medium, indicating the acquisition of spontaneous suppressors. Three suppressor strains of homo-40S were colony purified. All of them exhibited substantially improved growth rates in paromomycin-containing medium, and two of three suppressor strains displayed obviously decreased growth rates in yeast extract–peptone–dextrose (YPD) medium (*SI Appendix*, Fig. S9), indicating that they might have sacrificed fitness in YPD medium for improving paromomycin tolerance. WGS analysis was performed to determine the suppressor mutations, and three unique missense mutations in yeast protein kinase (Ypk1p), secretory protein 13 (Sec13p), and secretory protein 23 (Sec23p) were identified. Then, we constructed suppressor mutations in homo-40S and evaluated the effects of such mutations on paromomycin tolerance. As shown in Fig. 5*A*, these mutations

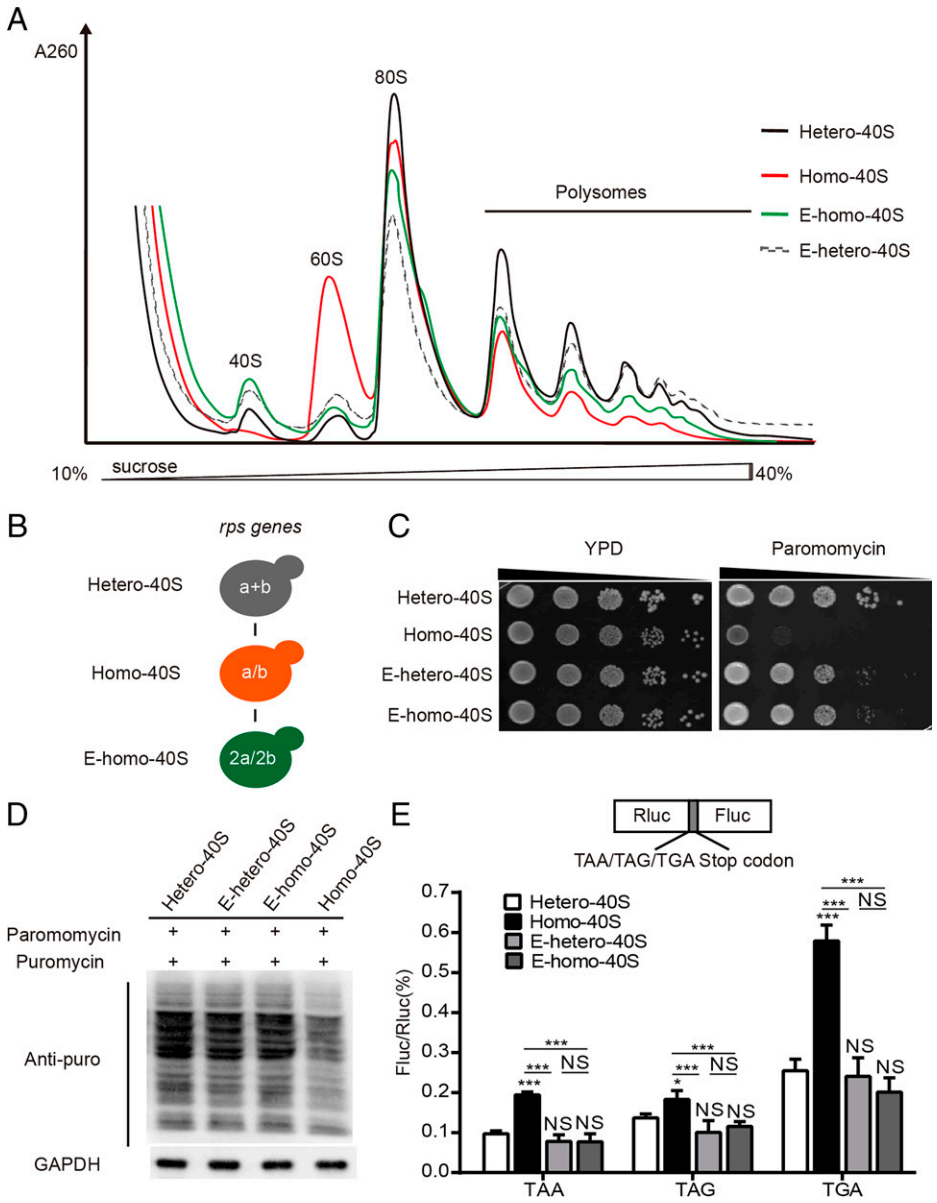

Fig. 4. Doubling of retained RP paralogous genes in homo-40S markedly rescues fitness and translational functionalities. (*A*) Overlay of polysome profiles from wild-type hetero-40S (black solid line), homo-40S (red solid line), E-hetero-40S (gray dotted line), and E-homo-40S (green solid line). (*B*) A schematic showing 40S RP gene compositions in wild-type or engineered cells. (*C*) Serial dilution assays of hetero-40S, homo-40S, E-hetero-40S, and E-homo-40S in the presence or absence of paromomycin. (*D*) Global translation rates were measured by puromycin incorporation. Neosynthesized proteins were labeled with puromycin and analyzed by immunoblotting with an antibody to puromycin. GAPDH is shown as a loading control. (*E*) The translation fidelities of wild type (hetero-40S), homo-40S, E-hetero-40S, and E-homo-40S were evaluated with reporters containing an insertion of a stop codon (TAA/TAG/TGA) between Rluc and Fluc. Values are represented as means ± SD (*t* test; ***$P < 0.001$; *$P < 0.05$; $n \geq 3$); NS, not significant.

(Ypk1p T502I, Sec13p G176R, and Sec23p S310F) resulted in weakened sensitivity of homo-40S to paromomycin. Consistently, a puromycin incorporation assay demonstrated that these gene mutations obviously improved the protein synthesis activity of homo-40S upon paromomycin treatment (Fig. 5*B* and *SI Appendix*, Fig. S10*A*). Previous studies reported that impairment of paromomycin uptake or sequestration of the drug in the vesicular cytoplasmic compartment could reduce the effective dose of drug acting on the ribosome and contribute to increased paromomycin resistance (26–28). Among these three suppressor genes, Ypk1p is a sphingoid base-regulated kinase and is required for endocytosis, which is critical for paromomycin uptake (27, 29). Notably, a previous study showed that T504, located close to T502 identified in our suppressor screening, was important for the endocytic function of Ypk1p (29). To investigate the role of Ypk1p T502I in endocytosis, we assayed the ability of cells to deliver lucifer yellow (LY) to the vacuole (Fig. 5*C*). The Ypk1p T502I suppressor strain displayed a strong defect in the accumulation of LY in the vacuole, indicating that the T502I mutation of Ypk1p impaired endocytosis, which consequently restricted the internalization of paromomycin and led to improved paromomycin tolerance. Although Sec23p is also involved in endocytosis (30), homo-40S with Sec23p S310F or Sec13p G176R mutations led to normal internalization of LY (*SI Appendix*, Fig. S10*B*), indicating that Sec23p S310F or Sec13p G176R improved paromomycin resistance via an endocytosis-independent pathway. Sec23p and Sec13p are the core

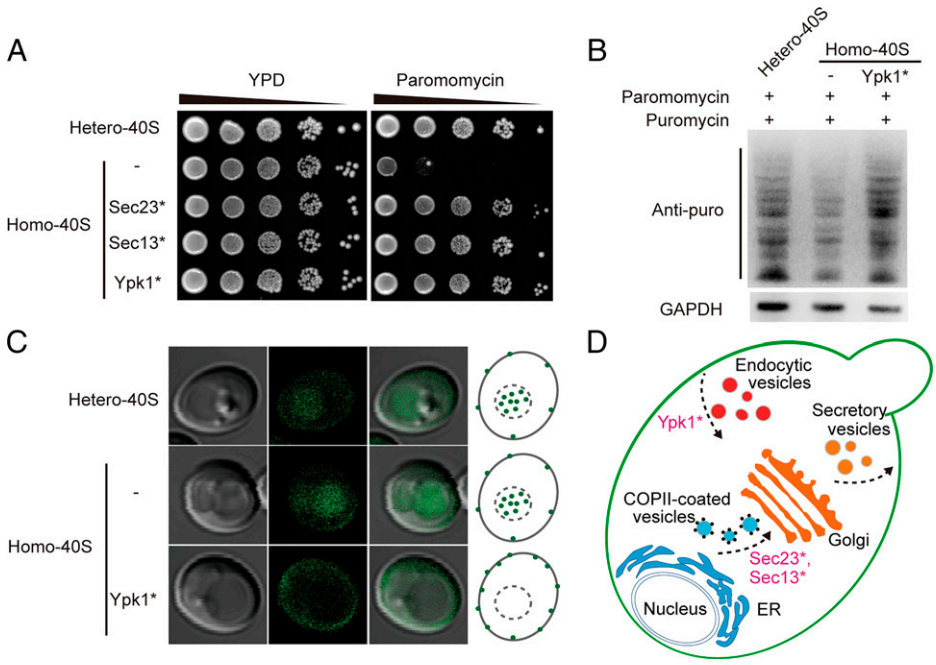

Fig. 5. Homo-40S adapts paromomycin via acquisition of bypass mutations. (*A*) Serial dilution assays of hetero-40S, homo-40S, and suppressor strains in the presence or absence of paromomycin; Sec23*, Sec23p S310F; Sec13*, Sec13p G176R; Ypk1*, Ypk1p T502I. (*B*) Global translation rates were measured by puromycin incorporation. Neosynthesized proteins were labeled with puromycin and analyzed by immunoblotting with antibody to puromycin. GAPDH is shown as a loading control. (*C*) Suppressor genes were mapped onto vesicular trafficking systems. (*D*) Endocytosis of LY was assayed in strains as indicated.

structural proteins of coat protein complex 2 (COPII) vesicles, and Sec23p S310F or Sec13p G176R may affect the structure of COPII vesicles (31). However, how paromomycin resistance is improved by these mutations of COPII vesicle-associated structural proteins is not well understood. Collectively, these results suggest that homo-40S could evolve to adapt to paromomycin via acquisition of bypass mutations that affect the surrounding gene networks, such as endocytosis and COPII vesicle-associated genes (Fig. 5*D*).

Homo-40S Evolved to be Diploid during Long-Term Culturing. Furthermore, to determine the long-term effect of the engineered homogeneous 40S ribosomal subunit on yeast cells, homo-40S cells were cultured to stationary phase and inoculated into fresh medium at a 1:100 dilution 20 times (Fig. 6*A*). The two fastest-growing evolved strains, evolver1 and evolver2, were isolated from the two independent evolved pools. Both evolved isolates outperformed the pre-evolved homo-40S strains (Fig. 6*B*), albeit without obvious restoration of paromomycin tolerance and translation fidelity (*SI Appendix*, Fig. S11), indicating that some genetic changes were acquired in the evolved strains. Although the pulsed-field gel electrophoresis results of the evolved isolates showed normal chromosome size (*SI Appendix*, Fig. S12), WGS and Sanger sequencing revealed that both evolved isolates had recurrent heterozygous mutations scattered across different chromosomes, indicating that the chromosome numbers of the evolved strains probably deviated from the normal ones (Fig. 6*C* and *SI Appendix*, Fig. S13). Cellular DNA contents were therefore stained with propidium iodide (PI) and measured by flow cytometry. The evolved isolates displayed doubled DNA contents of homo-40S, suggesting that genome duplication events occurred during long-term culture. (Fig. 6*D*). By contrast, no genome duplication events were observed in the evolved isolates from hetero-40S, E-hetero-40S, and E-homo-40S after the same long-term culturing as homo-40S (*SI Appendix*, Fig. S14). To further examine whether genome duplication contributed to the phenotypic restoration of the evolved isolates, a diploid homo-40S strain (i.e., di-homo-40S) was constructed through mating of haploid homo-40S. In addition, di-homo-40S showed an obviously improved growth rate, to a level comparable to that of the evolved strains (Fig. 6*B* and *SI Appendix*, Fig. S11), which supports the conjecture that homo-40S could evolve to be diploid to improve its growth robustness.

Discussion

Although numerous studies have previously presented a wealth of evidence showing RP specificity and potential for specialized ribosomes in diverse organisms (e.g., *Escherichia coli*, yeast, *Dictyostelium*, *Arabidopsis*, zebrafish, and mice), the functional significance of pervasive RP paralogs, especially their roles in customizing translation abilities, remains poorly understood and is the subject of focused attention (5–7). Characterization of monotypic ribosomes with specific and homogeneous RP paralog compositions was straightforward and could be an ideal approach to answer these questions. Unfortunately, given the complexity of the cellular ribosome pool (e.g., in *S. cerevisiae*, 59 RP paralog pairs allow $>10^{17}$ potential RP combinations) and the high similarity of RP paralogs, it was almost impossible to isolate monotypic ribosomes from the enormously varied ribosome population for further functional characterization (5, 6).

While previous studies have characterized strains with simplified cellular ribosome pools by deleting one or both paralogs for a single RP, the extreme case of simplification, namely engineering monotypic ribosomes consisting of homogeneous RP paralogs, is of great significance and remains to be explored (5–7). In this work, we reported an iterative genome-editing method (iCasEvo) based on the CRISPR–Cas9 system for gene editing and a PEE for curing gRNA-expressing plasmids with >95% efficiency, which provided an effective tool to delete 24 40S RP paralogous genes sequentially. More generally, iCasEvo could contribute to further strain engineering, which usually

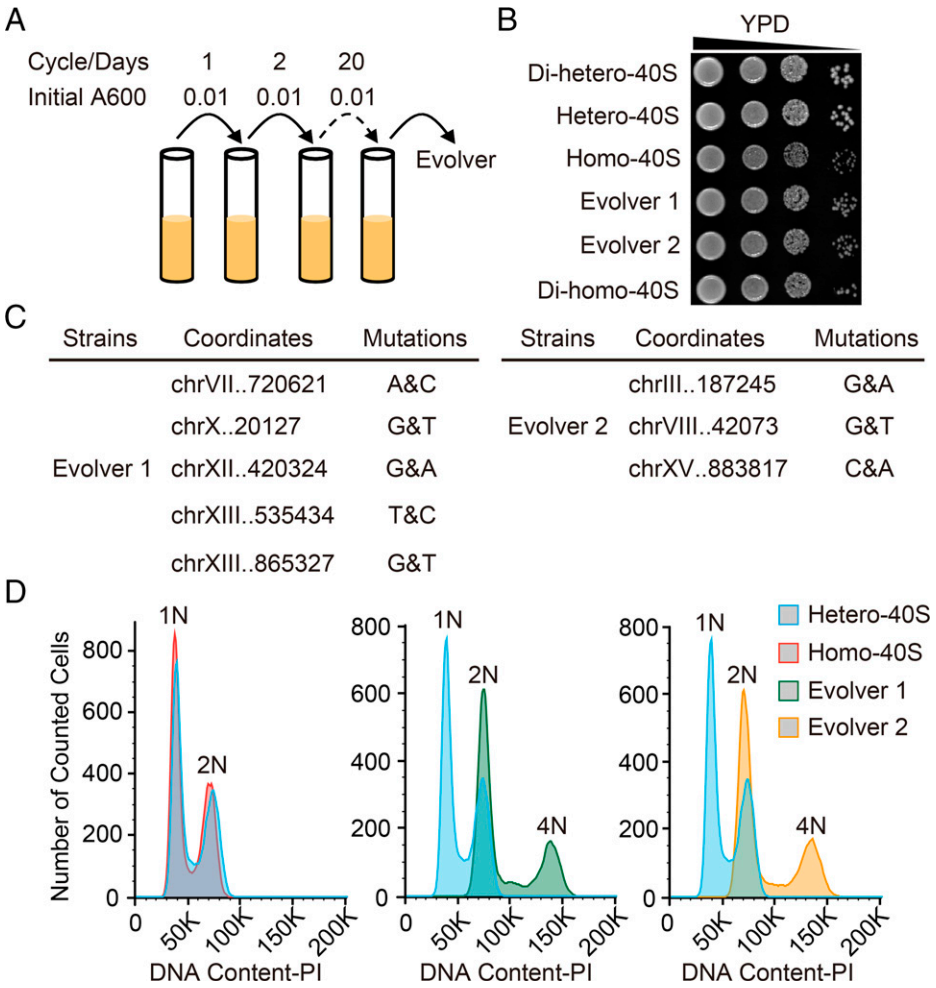

Fig. 6. Homo-40S evolved to be diploidy during long-term culturing. (*A*) Diagram showing how homo-40S strains were evolved for 20 cycles in liquid medium (YPD). (*B*) Serial dilution assays with diploid or haploid wild-type (di-hetero-40S or hetero-40S), synthetic homo-40S, two evolved isolates (evolver 1 and evolver 2), and diploid homo-40S (di-homo-40S). (*C*) WGS identified recurrent heterozygous mutations in evolved isolates. (*D*) Strains were analyzed for haploidy or diploidy by measuring DNA intensity by fluorescence-activated cell sorting (FACS). Chromosome ploidy of tested strains was normalized to the haploid wild-type (hetero-40S), which showed N or 2N DNA content during mitotic growth.

requires large-scale genome modifications to achieve specific phenotypes. For example, 14 successive rounds of gene editing were carried out to fuse 16 yeast chromosomes into a single chromosome (16), and 26 genomic modifications were necessary to optimize the microbial production of 1,3-propanediol (32). With the aid of iCasEvo, we successfully simplified the heterogeneous cellular 40S ribosome pool into a more homogeneous form by deleting 24 RP paralogous genes, which provided an effective way to generate monotypic 40S consisting of defined and homogeneous RP paralogs.

Comparative analysis of the engineered homo-40S and the wild-type strain revealed that systematic deletion of the 24 RP paralogs led to only mild loss of growth robustness under nutrient-rich culturing conditions and under most of the stress conditions, indicating that these deleted RP paralogs played a minor role in maintaining cell viability or growth robustness under these conditions. Consistent with this phenotype, no obvious changes in global translational activity were observed for homo-40S. The reason may be that only "subordinate" paralogous genes were selected for deletion in homo-40S, while translation is mostly performed by ribosomes comprising the "major" paralogs (2). Previous studies reported that deletions or mutations in certain 40S RP genes (*rps2* or *sup44*, *rps13* or *sup46*, *rps18a*, and *rps28a*) led to substantially increased sensitivity to the translation error-inducing inhibitor paromomycin and reduced translational fidelity in yeast (33–36). In our study, while these RP genes were reserved in homo-40S, homo-40S displayed hypersensitivity to the translation error-inducing inhibitor paromomycin, obviously decreased translational activity upon paromomycin treatment, and significantly increased stop codon readthrough, indicating that these "subordinate" RP paralogs also functioned in fine-tuning translational functionalities with regard to translational fidelity and activity. In theory, these types of phenotypic changes in homo-40S may result from a decrease in total functional ribosomes (dose effects), the loss of specialized ribosomes critical to tune these translational properties ("specialized ribosome" effects), or both (37). The fact that these phenotypes of homo-40S caused by loss of RP alternatives were partially reversed by doubling of the remaining RP paralogous genes not only highlighted the effects of gene dose but also hinted at the existence of the "specialized ribosomes" effect. To directly evaluate the "specialized ribosome" effect, it is worth further comparative analysis of different monotypic 40S subunits with distinct RP paralog contents (e.g., the monotypic 40S comprising the "major" RP paralogs versus 40S comprising "subordinate" RP paralogs).

Intriguingly, homo-40S rapidly obtained paromomycin tolerance and improved growth robustness through spontaneous

genetic changes. Although paromomycin acts to inhibit protein synthesis through its interaction with 40S ribosome subunits, our further analysis of paromomycin-resistant derivatives of homo-40S highlighted endocytosis- and COPII vesicle-associated genes, including *ypk1*, *sec23*, and *sec13*. Missense mutations of these genes (Ypk1p T502I, Sec23p S310F, and Sec13p G176R) led to increased translation activity and paromomycin tolerance. Among them, Ypk1p has been reported to be required for endocytosis, which is critical for the internalization of paromomycin (27, 29). Consistent with previous studies, the Ypk1p T502I strain showed substantially reduced endocytosis, indicating that the impaired uptake of paromomycin consequently led to improved paromomycin tolerance. In contrast, Sec23p S310F and Sec13p G176R did not obviously affect endocytosis. Indeed, Sec23p and Sec13p are well known as core coat proteins of COPII vesicles implicated in protein transport from the endoplasmic reticulum (ER) to the Golgi. Our suppressor screening enriched two separate protein components of COPII vesicles, implying that adjustments of COPII vesicles contribute to paromomycin resistance. The link between mutations of COPII components and increased paromomycin resistance remains to be established. Since the vesicular sequestration of drugs is a well-known mechanism of drug resistance (28, 38, 39), future work might provide additional mechanistic insights by comparing the paromomycin sequestration activity between wild-type COPII vesicles and vesicles with Sec23p S310F and/or Sec13p G176R. Additionally, previous studies reported that Sec13p was also one of the essential subunits of the Nup84p nuclear pore subcomplex that contributed to the transcriptional activation of RP genes (40, 41). Since Sec13p G176R improved the translational incorporation of puromycin in homo-40S (*SI Appendix*, Fig. S9*A*), further evaluation of the effects of the Sec13p G176R mutation on RP and ribosome synthesis might provide additional explanation that Sec13p G176R might up-regulate RP synthesis to compensate the RP dosage loss in homo-40S. In addition to small-scale genomic variations, during long-term culture, homo-40S evolved to duplicate its genome, resembling the early evolutionary trajectory of yeasts, to acquire higher growth rates (8, 9), highlighting the plasticity of yeast to accommodate to environmental and genetic changes. Diploidization of haploid yeast can be generally caused by mating-type switching followed by mating or DNA replication without subsequent cell division. As the gene encoding homing endonuclease enzyme (HO), essential for mating-type switching, was inactivated by *cas9* gene insertion in homo-40S, mating-type switch of homo-40S would be an extremely rare event (42). Consistent with this, both evolver1 and evolver2 showed mating type a (MATa), the same mating type as homo-40S (*SI Appendix*, Fig. S15). Therefore, DNA synthesis without division (division deficiency) was more likely the mechanism behind diploidy of homo-40S. However, how RP deletions are correlated to the division deficiency of homo-40S is still unclear and remains to be addressed in the future.

In conclusion, our work provided an effective method to engineer yeast with monotypic 40S ribosomes, including both defined and homogenous RP paralogs. Further functional studies revealed that the "subordinate" RP paralogs played a minor role in normal translation to maintain growth robustness but functioned in fine-tuning translation to acquire phenotypic plasticity (such as paromomycin tolerance) through dose compensation and the posited specialized function. This study provided proof of principle for the feasibility of functionally dissecting the pervasive and heterogenous RP paralogs through engineering and characterizing of yeasts with monotypic ribosomes. In the future, our approach may possibly be used to engineer customized ribosomes by varying RP paralog contents to provide additional insights into the specialized functions of ribosomes (6, 7) or, more generally, to facilitate engineering other variants with combinatorial genome modifications (16, 32).

Materials and Methods

Strains. All strains used in this study are listed in Dataset S2. They are all derivatives of BY4741 (*MATa his3*Δ0 *leu2*Δ0 *met15*Δ0 *ura3*Δ0). The Sec23p G176R mutation in homo-40S was constructed by two-step PCR-based homologous recombination. The deletion cassette of *his3* flanked by homologous left (HL) and homologous right (HR) arms was obtained by extension PCR. Genomic DNA of homo-40S suppressor was used as PCR template for amplification of the *sec23* mutation sequence. PCR primers used to construct the Sec23p G176R mutation are described in Dataset S2. Ypk1p T502I and Sec13p G176R mutations in homo-40S were constructed by iCasEvo, as described in *Materials and Methods*.

Plasmid Constructions. For Cas9 expression, a codon-optimized version of the *Streptococcus pyogenes* Cas9 gene fused to a simian virus 40 (SV40) nuclear localization sequence was cloned into an integration cassette under the expression of the strong glyceraldehydes-3-phosphate dehydrogenase (GAP) promoter with a cytochrome C1 (CYC1) terminator (13). For gRNA cassette construction, targeting gRNAs were cloned into the generic gRNA cassettes in between the hepatitis delta virus (HDV) ribozyme and structural RNAs flanked by the small nucleolar RNA 52 (SNR52) polymerase III promoter and a Suppressor 4 (SUP4) terminator in the pRS4XX-series 2μ vector (43). The target sequences of gRNAs were manually selected from the open reading frame or introns of genes to be deleted. Donor cassettes with 200 to 500 base pairs (bp) of flanking homology were generated by PCR amplification and ligated together by Golden Gate Assembly. To construct vector cassettes, structural RNA with 20-bp 2μ-targeted gRNA flanked with the hammerhead (HH) and the HDV ribozymes were synthesized using overlap extension PCR (OE-PCR) and cloned into the pRS4XX-series 2μ vectors under the control of the inducible pGalS promoter and a CYC1 terminator. For the dual-luciferase assay, coding sequences of Rluc and Fluc were synthesized using OE-PCR and driven by the same promoters and terminators as previously reported (22–24). All plasmids used in this study are listed in Dataset S2.

iCasEvo. gRNA/donor/vector cassettes were PCR amplified separately (50-μL PCR reactions each) with generic primers listed in Dataset S2 and cotransformed into *S. cerevisiae* using a standard lithium acetate (LiOAc) transformation protocol (17). The colonies growing on the selective plates were streaked onto the fresh selective plates and then subjected to PCR analysis to verify the deletion of the targeted genes. After verification, the positive colonies were streaked onto yeast extract–peptone (YEP)–galactose plates (complete medium with 2% galactose as a carbon source) to remove the editing cassettes. Next, the single colonies were replicated onto selective or complete medium and further verified by PCR analysis before the next round of gene deletion to ensure the successful deletion of genes and elimination of editing cassettes.

Pulsed-Field Gel Electrophoresis. Plug samples were resolved on a 0.9% agarose gel in 0.5× Tris–borate–ethylenediaminetetraacetic acid (TBE) for 23 h at 14 °C on a Bio-Rad CHEF Mapper XA Pulsed Field Electrophoresis System. The voltage was 5.5 V/cm at an angle of 120°, and a switch time from initial 50 s to final 2 min was used.

Serial Dilution Assays. Single colonies were cultured in liquid YPD overnight at 30 °C. Cell density was adjusted to the same optical density at 600 nm (OD_{600}) and series diluted by 10-fold. Then, the dilutions were spotted onto various selective plates and incubated at 30 °C. For carbon source usage analysis, cells used 2% galactose or 3% glycerol instead of the 2% glucose as carbon sources. For stress treatment, cells were cultured in YPD medium containing 2 μg/mL Nocodazole, 8 mM dithiothreitol (DTT), 1 M NaCl, 6% ethanol, 0.3% acetic acid, 5 μg/mL anisomycin, 35 μg/mL hygromycin B, or 1 mg/mL paromomycin separately.

Growth Curve and Doubling Time Assay. Growth curve measurements by microcultivation were performed as previously described (44). Briefly, the log-phase cells were centrifuged and resuspended with fresh medium with or without stresses to get a starting OD_{600} of 0.05. One hundred microliters of cell culture was added to each well of Costar clear polystyrene 96-well plates. Three or four biological replicates were analyzed for each strain. The 96-well plate was sealed with Breathe-Easy membrane (Sigma, lot number MKBZ0331) and then cultivated in an Epoch2 microplate photometer (BioTek) at 30 °C for 36 h for YPD and for 72 h for stress conditions. The OD_{600} values of cultures were recorded every 10 min after 30 s of shaking at 282 rpm. The data were analyzed using the GraphPad Prism 8 software to generate growth

curves and doubling time. Concentrations for liquid microcultivation were as follows: 2% galactose, 3% glycerol, 2 μg/mL Nocodazole, 8 mM DTT, 1 M NaCl, 6% ethanol, and 0.3% acetic acid.

Construction of the Synthetic RP Gene Cluster. The designed synthetic RP gene cluster was originated from 24 individual RP gene cassettes (listed in Dataset S2), which were PCR amplified and cloned into the pUC19 plasmid. Each RP gene cassette was flanked by two recognition sites of Type IIS restriction enzymes (BsaI or BsmBI), and six or seven were pooled together to perform Golden Gate Assembly and cloned into an acceptor vector to obtain the new plasmid. The assembled plasmids were digested with NotI-high fidelity (NotI-HF) (NEB, R0198) and cotransformed into yeast to construct the gene cluster through the robust homologous recombination system.

Genomic DNA Preparation for PCR Analysis and DNA Sequencing. Five milliliters of overnight culture was collected and resuspended in 200 μL of breaking buffer (2% [vol/vol] Triton X-100, 1% [wt/vol] sodium dodecyl sulfate [SDS], 100 mM NaCl, 10 mM Tris-HCl pH 8.0, and 1 mM ethylenediaminetetraacetic acid [EDTA] pH 8.0). Cells were then mixed with 200 μL of phenol/chloroform/isoamyl alcohol (25:24:1) and 200 μL of glass beads (Biospec, 11079105) and vortexed at 2,000 rpm for 10 min. The mix was added to 200 μL of double-distilled water (ddH_2O), followed by centrifugation at 12,000 rpm for 10 min. Then, the top layer was collected and deposited with 1 mL of 100% ethanol. After drying in a vacuum pump, the pellet was resuspended in 0.4 mL of sterile water and was ready for PCR verification. For DNA sequencing, DNA was incubated with 10 μL of 10 mg/mL RNase for 1 h at 37 °C and mixed with 4 μL of 4 M ammonium acetate and 1 mL of 100% ethanol, followed by centrifugation for 15 min at 12,000 rpm. Finally, the genomic DNA was dissolved in 100 μL of sterile water for genome-sequencing analysis.

WGS Analysis. The quality of the raw reads was first evaluated with FastQC (https://www.bioinformatics.babraham.ac.uk/projects/fastqc/), and then low-quality reads were excluded using Trimmomatic (0.36) with default parameters (45). After that, the cleaned reads were mapped to the reference genome of yeast (SGD; https://www.yeastgenome.org) with Bwa (v0.7.12) (46). Then, Picard tools (v1.119; https://broadinstitute.github.io/picard/) were used to covert the sam file to a bam file and to remove the duplicated reads caused by PCR amplification. RealignerTargetCreator and IndelRealigner of the Genome Analysis Toolkit (GATK v3.5) were used to realign the reads around the insertion–deletion mutations (indels) to reduce the errors of SNP calling near the indels (47). Finally, SNPs were identified by the HaplotypeCaller program of GATK and annotated with SnpEff (48) and were further validated by Sanger sequencing. Raw sequence reads are available at NCBI BioProject PRJNA707077.

RNA Preparation for mRNA Sequencing and Transcriptomic Analysis. Total RNA was extracted by using the RNAprep Pure Plant Plus kit (polysaccharides & polyphenolics-rich; DP441, QIAGEN, Germany). RNA integrity was controlled using the RNA Nano 6000 Assay kit of the Bioanalyzer 2100 system (Agilent Technologies, CA, USA). Complementary DNA (cDNA) library fragments and PCR products were purified with the AMPure XP system (Beckman Coulter, Beverly, USA). Library quality was assessed on the Agilent Bioanalyzer 2100 system. Clustering of the index-coded samples was performed on a cBot Cluster Generation System using a TruSeq PE Cluster kit v3-cBot-HS (Illumina) according to the manufacturer's instructions. After cluster generation, the library preparations were sequenced on an Illumina NovaSeq platform. Clean data were obtained by removing reads containing adapter, ploy-N, and low-quality reads from raw data. Paired-end clean reads were aligned to the reference genome using Hisat2 v2.0.5. Reference genomes were from https://ftp.ncbi.nlm.nih.gov/genomes/all/GCF/000/146/045/GCF_000146045.2_R64/. Differential expression analysis of two groups (three biological replicates per condition) was perform using the DESeq2R package (1.20.0). The resulting *P* value were adjusted using Benjamini and Hochberg's approach for controlling the false discovery rate. The differentially expressed genes were displayed with a *P* value of ≤ 0.01 and a $\log_2$ fold change of ≥ 1. GO enrichment analysis of differentially expressed gene was implemented by the clusterProfiler R package. Raw sequence reads are available at NCBI BioProject PRJNA773207.

Dual-Luciferase Assay. Yeast cells with reporter plasmids were cultured overnight in liquid selective medium at 30 °C. The culture was diluted to the starting OD_{600} of 0.1 with fresh medium and collected at an OD_{600} of ~0.7. Cells were washed three times with cold phosphate-buffered saline (PBS) (pH 7.4) with 1 mM phenylmethylsulfonyl fluoride (PMSF), resuspended in 300 μL of the same buffer, and mixed with 300 μL of glass beads. Then the samples were vortexed for 10 s with the bead beater and cooled on ice for 20 s with 60 cycles. After centrifugation for 10 min at 12,000 rpm, the supernatants were collected. Luciferase activity was measured by the Dual-Luciferase Reporter Assay System (Promega, PR-E1910). Each experiment was performed with a minimum of three biological replicates. The results were represented as the ratio of Fluc to Rluc activity, and statistical analysis of the results was performed by Student's *t* test.

Ribosome Profile Analysis. The culture was diluted to the starting OD_{600} of 0.1 with fresh medium and collected by centrifugation at an OD_{600} of ~0.8. Cells were resuspended with cold buffer (20 mM Tris-HCl [pH 7.5], 100 mM NH_4Cl, 0.5 mM $MgCl_2$, and 1 mM DTT) with 1 mM PMSF and disrupted by ultrasonication. The lysate was centrifuged at 15,000 rpm (Avanti J-26 XP, Beckman Coulter) for 1 h. Then, the supernatants were loaded onto a 10 to 40% sucrose gradient and centrifuged at 39,000 rpm in an SW41 rotor (Beckman Coulter) for 3.5 h at 4 °C. The fractions were analyzed by a Teledyne ISCO fractionation system with A254 absorbance.

Microscope Imaging for Cell Morphology. Cells from single colonies were cultured in YPD overnight and subcultured into fresh medium (starting OD_{600} = 0.1) for another 5 h. Cells were centrifuged gently and washed once with ddH_2O. Then, cells were dropped on slides for further imaging with a Nikon A1 confocal microscope under a ×60 objective.

Uptake Assay of LY. Cells from single colonies were cultured in YPD overnight and subcultured into fresh medium (starting OD_{600} = 0.2) for another 4 h. About 3×10^6 cells were harvested and resuspended in 100 μL of YPD with 4 mg/mL LY. After incubation with LY for 1 h at room temperature, cells were harvested by centrifugation at 2,000 rpm for 2 min. Cells were washed with 1 mL of ddH_2O and resuspended in 20 μL of ddH_2O. Then, cells were dropped on slides for further imaging with a Nikon A1 confocal microscope under a ×60 objective.

Western Blot Analysis. For puromycin incorporation, overnight cultures were diluted to an OD_{600} of 0.1 to 0.2 with 5 mL of fresh medium with or without 1 mg/mL paromomycin (Solarbio, P8230) treatment for 6 h and grown to log phase. Puromycin was added directly to the culture at a final concentration of 2 mM and incubated 1 h at 30 °C. Then, two OD_{600} cells were collected and lysed by alkaline lysis. The sediment was suspended in SDS buffer (60 mM Tris-HCl [pH 6.8], 10% glycerol, 2% SDS, 0.01% bromophenol blue, 0.01 M DTT, and 5% β-mercaptoethanol) and heated at 100 °C for 10 min. The protein samples were collected form the supernatant after centrifuging. Equal volumes of protein samples were separated on 10% SDS-polyacrylamide gel electrophoresis (PAGE) gels, followed by detection of puromycin-incorporated proteins with the anti-puromycin monoclonal antibody (Merck, MABE343). Equal loading was controlled by the protein level of glyceraldehyde 3-phosphate dehydrogenase (GAPDH) (ABclonal, AC033).

Flow Cytometry Analysis of Yeast Strains. Cells from single colonies were cultured in YPD overnight and subcultured into fresh medium (starting OD_{600} = 0.1) for another 5 h. Cells (5×10^6) were centrifuged and then fixed with 70% ethanol overnight at 4 °C. Cells were pelleted and resuspended in 50 mM sodium citrate (pH 7.0). Then, cells were sonicated briefly on ice, pelleted, and resuspended in 50 mM sodium citrate (pH 7.0). RNaseA was added to the cells (0.25 mg/mL) and incubated overnight at 37 °C. Cells were then washed with 50 mM sodium citrate (pH 7.0) and resuspended into the same solution. PI (16 μg/mL) was added to the cells and incubated at room temperature for 30 min. Samples were then analyzed with a BD FACSCelesta.

Mating-Type Switch and Preparation of Diploid Strains. Plasmids carrying inducible HO endonuclease were transformed into a haploid yeast strain. The cells with plasmids were cultured in 5 mL of synthetic complete medium without leucine (SC-LEU) with 2% glucose medium at 30 °C overnight. The overnight culture was diluted to an OD_{600} of 0.1 using 3 mL of SC-LEU with 2% raffinose/0.1% glucose and cultured at 30 °C for 4 h. Galactose was added to the cells to make the final concentration 2%. Cells were cultured at 30 °C for 2 h to induce HO. Then, the cells were diluted and plated onto YPD plates. Single colonies without plasmids but with the desired mating type were chosen for further cross with the original haploid strain. After cross on YPD plates for about 4 h, zygotes were isolated from the mating mixture with a micromanipulator. Zygotes were cultured for 2 d at 30 °C before mating-type testing with tester strains.

Data Availability. Raw sequence reads are available at NCBI BioProject under accession nos. PRJNA707077 and PRJNA773207. All other study data are included in the article and/or supporting information.

ACKNOWLEDGMENTS. The authors are grateful to Wen Wang, Qiang Qiu, Ning Gao, and members of the G.Z. and J.D. laboratories for helpful and constructive suggestions at various stages of this work. This work was supported

by the National Key Research and Development Program of China (2017YFA0505103), National Natural Science Foundation of China (31725002, 31971340, 31800080, and 8190107), Shenzhen Science and Technology Program (KQTD20180413181837372), Guangdong Provincial Key Laboratory of Synthetic Genomics (2019B030301006), and Shenzhen Outstanding Talents Training Fund.

1. M. B. Ferretti, H. Ghalei, E. A. Ward, E. L. Potts, K. Karbstein, Rps26 directs mRNA-specific translation by recognition of Kozak sequence elements. *Nat. Struct. Mol. Biol.* **24**, 700–707 (2017).
2. M. M. Ghulam, M. Catala, S. Abou Elela, Differential expression of duplicated ribosomal protein genes modifies ribosome composition in response to stress. *Nucleic Acids Res.* **48**, 1954–1968 (2020).
3. N. Segev, J. E. Gerst, Specialized ribosomes and specific ribosomal protein paralogs control translation of mitochondrial proteins. *J. Cell Biol.* **217**, 117–126 (2018).
4. Z. Shi *et al.*, Heterogeneous ribosomes preferentially translate distinct subpools of mRNAs genome-wide. *Mol. Cell* **67**, 71–83 (2017).
5. E. Emmott, M. Jovanovic, N. Slavov, Ribosome stoichiometry: From form to function. *Trends Biochem. Sci.* **44**, 95–109 (2019).
6. N. R. Genuth, M. Barna, The discovery of ribosome heterogeneity and its implications for gene regulation and organismal life. *Mol. Cell* **71**, 364–374 (2018).
7. J. E. Gerst, Pimp my ribosome: Ribosomal protein paralogs specify translational control. *Trends Genet.* **34**, 832–845 (2018).
8. M. Kellis, B. W. Birren, E. S. Lander, Proof and evolutionary analysis of ancient genome duplication in the yeast *Saccharomyces cerevisiae*. *Nature* **428**, 617–624 (2004).
9. K. H. Wolfe, D. C. Shields, Molecular evidence for an ancient duplication of the entire yeast genome. *Nature* **387**, 708–713 (1997).
10. J. D. Dinman, Pathways to specialized ribosomes: The Brussels Lecture. *J. Mol. Biol.* **428** (10 Pt B), 2186–2194 (2016).
11. Z. Shi, M. Barna, Translating the genome in time and space: Specialized ribosomes, RNA regulons, and RNA-binding proteins. *Annu. Rev. Cell Dev. Biol.* **31**, 31–54 (2015).
12. S. Xue, M. Barna, Specialized ribosomes: A new frontier in gene regulation and organismal biology. *Nat. Rev. Mol. Cell Biol.* **13**, 355–369 (2012).
13. A. A. Horwitz *et al.*, Efficient multiplexed integration of synergistic alleles and metabolic pathways in yeasts via CRISPR-Cas. *Cell Syst.* **1**, 88–96 (2015).
14. S. Komili, N. G. Farny, F. P. Roth, P. A. Silver, Functional specificity among ribosomal proteins regulates gene expression. *Cell* **131**, 557–571 (2007).
15. K. K. Steffen *et al.*, Ribosome deficiency protects against ER stress in *Saccharomyces cerevisiae*. *Genetics* **191**, 107–118 (2012).
16. Y. Shao *et al.*, Creating a functional single-chromosome yeast. *Nature* **560**, 331–335 (2018).
17. W. Zhang *et al.*, Engineering the ribosomal DNA in a megabase synthetic chromosome. *Science* **355**, eaaf3981 (2017).
18. E. K. Schmidt, G. Clavarino, M. Ceppi, P. Pierre, SUnSET, a nonradioactive method to monitor protein synthesis. *Nat. Methods* **6**, 275–277 (2009).
19. K. Fujii, T. T. Susanto, S. Saurabh, M. Barna, Decoding the function of expansion segments in ribosomes. *Mol. Cell* **72**, 1013–1020 (2018).
20. N. Garreau de Loubresse *et al.*, Structural basis for the inhibition of the eukaryotic ribosome. *Nature* **513**, 517–522 (2014).
21. I. Prokhorova *et al.*, Aminoglycoside interactions and impacts on the eukaryotic ribosome. *Proc. Natl. Acad. Sci. U.S.A.* **114**, E10899–E10908 (2017).
22. J. W. Harger, J. D. Dinman, Evidence against a direct role for the Upf proteins in frameshifting or nonsense codon readthrough. *RNA* **10**, 1721–1729 (2004).
23. E. B. Kramer, H. Vallabhaneni, L. M. Mayer, P. J. Farabaugh, A comprehensive analysis of translational missense errors in the yeast *Saccharomyces cerevisiae*. *RNA* **16**, 1797–1808 (2010).
24. K. L. Muldoon-Jacobs, J. D. Dinman, Specific effects of ribosome-tethered molecular chaperones on programmed -1 ribosomal frameshifting. *Eukaryot. Cell* **5**, 762–770 (2006).
25. X. Escalera-Fanjul, H. Quezada, L. Riego-Ruiz, A. González, Whole-genome duplication and yeast's fruitful way of life. *Trends Genet.* **35**, 42–54 (2019).
26. B. Chawla, A. Jhingran, A. Panigrahi, K. D. Stuart, R. Madhubala, Paromomycin affects translation and vesicle-mediated trafficking as revealed by proteomics of paromomycin -susceptible -resistant *Leishmania donovani*. *PLoS One* **6**, e26660 (2011).
27. A. Jhingran, B. Chawla, S. Saxena, M. P. Barrett, R. Madhubala, Paromomycin: Uptake and resistance in *Leishmania donovani*. *Mol. Biochem. Parasitol.* **164**, 111–117 (2009).
28. D. L. Kramer, J. D. Black, H. Mett, R. J. Bergeron, C. W. Porter, Lysosomal sequestration of polyamine analogues in Chinese hamster ovary cells resistant to the *S*-adenosylmethionine decarboxylase inhibitor, CGP-48664. *Cancer Res.* **58**, 3883–3890 (1998).
29. A. K. deHart, J. D. Schnell, D. A. Allen, L. Hicke, The conserved Pkh-Ypk kinase cascade is required for endocytosis in yeast. *J. Cell Biol.* **156**, 241–248 (2002).
30. E. Peñalver, P. Lucero, E. Moreno, R. Lagunas, Clathrin and two components of the COPII complex, Sec23p and Sec24p, could be involved in endocytosis of the *Saccharomyces cerevisiae* maltose transporter. *J. Bacteriol.* **181**, 2555–2563 (1999).
31. C. A. Kaiser, R. Schekman, Distinct sets of SEC genes govern transport vesicle formation and fusion early in the secretory pathway. *Cell* **61**, 723–733 (1990).
32. C. E. Nakamura, G. M. Whited, Metabolic engineering for the microbial production of 1,3-propanediol. *Curr. Opin. Biotechnol.* **14**, 454–459 (2003).
33. J. A. All-Robyn, N. Brown, E. Otaka, S. W. Liebman, Sequence and functional similarity between a yeast ribosomal protein and the *Escherichia coli* S5 ram protein. *Mol. Cell Biol.* **10**, 6544–6553 (1990).
34. R. A. Anthony, S. W. Liebman, Alterations in ribosomal protein RPS28 can diversely affect translational accuracy in *Saccharomyces cerevisiae*. *Genetics* **140**, 1247–1258 (1995).
35. L. S. Folley, T. D. Fox, Reduced dosage of genes encoding ribosomal protein S18 suppresses a mitochondrial initiation codon mutation in *Saccharomyces cerevisiae*. *Genetics* **137**, 369–379 (1994).
36. M. Masurekar, E. Palmer, B.-I. Ono, J. M. Wilhelm, F. Sherman, Misreading of the ribosomal suppressor SUP46 due to an altered 40 S subunit in yeast. *J. Mol. Biol.* **147**, 381–390 (1981).
37. E. W. Mills, R. Green, Ribosomopathies: There's strength in numbers. *Science* **358**, eaan2755 (2017).
38. A. B. Shapiro, K. Fox, P. Lee, Y. D. Yang, V. Ling, Functional intracellular P-glycoprotein. *Int. J. Cancer* **76**, 857–864 (1998).
39. M. A. Sognier *et al.*, Sequestration of doxorubicin in vesicles in a multidrug-resistant cell line (LZ-100). *Biochem. Pharmacol.* **48**, 391–401 (1994).
40. S. J. Deminoff, G. M. Santangelo, Rap1p requires Gcr1p and Gcr2p homodimers to activate ribosomal protein and glycolytic genes, respectively. *Genetics* **158**, 133–143 (2001).
41. B. B. Menon *et al.*, Reverse recruitment: The Nup84 nuclear pore subcomplex mediates Rap1/Gcr1/Gcr2 transcriptional activation. *Proc. Natl. Acad. Sci. U.S.A.* **102**, 5749–5754 (2005).
42. H. Meiron, E. Nahon, D. Raveh, Identification of the heterothallic mutation in HO-endonuclease of *S. cerevisiae* using HO/ho chimeric genes. *Curr. Genet.* **28**, 367–373 (1995).
43. O. W. Ryan *et al.*, Selection of chromosomal DNA libraries using a multiplex CRISPR system. *eLife* **3**, e03703 (2014).
44. Z. Luo *et al.*, Identifying and characterizing SCRaMbLEd synthetic yeast using ReSCuES. *Nat. Commun.* **9**, 1930 (2018).
45. A. M. Bolger, M. Lohse, B. Usadel, Trimmomatic: A flexible trimmer for Illumina sequence data. *Bioinformatics* **30**, 2114–2120 (2014).
46. H. Li, R. Durbin, Fast and accurate short read alignment with Burrows-Wheeler transform. *Bioinformatics* **25**, 1754–1760 (2009).
47. A. McKenna *et al.*, The Genome Analysis Toolkit: A MapReduce framework for analyzing next-generation DNA sequencing data. *Genome Res.* **20**, 1297–1303 (2010).
48. P. Cingolani *et al.*, A program for annotating and predicting the effects of single nucleotide polymorphisms, SnpEff: SNPs in the genome of *Drosophila melanogaster* strain w1118; iso-2; iso-3. *Fly (Austin)* **6**, 80–92 (2012).